SUPPLEMENTARY MATERIAL: Calibrated sub-micron temperature mapping of an operating plasmonic HAMR device by thermoreflectance imaging

Gregory T. Hohensee[1], Dustin Kendig[2], Ella Pek[3], Wan Kuang[1,4], Kazuaki Yazawa[2,5], and Ali Shakouri[5]

[1]Western Digital Corporation, 1250 Reliance Way, Fremont CA 94539, U.S.A.
[2]Microsanj LLC, 3287 Kifer Road, Santa Clara CA 95051, U.S.A.
[3]Department of Materials Science and Engineering, Materials Research Laboratory, University of Illinois at Urbana-Champaign, Urbana, IL 61801, U.S.A.
[4]Department of Electrical and Computer Engineering, Boise State University, Boise, ID 83725, U.S.A.
[5]Department of Electrical and Computer Engineering, Purdue University, West Lafayette, IN 47907, U.S.A.

TIME-RESOLVED THERMOREFLECTANCE IMAGING

We use stroboscopic imaging [1] to create time-resolved image data with temporal resolution down to 50 ns. The device is turned ON for a designated period of time at a designated duty cycle, and the CCD exposure time is also set by the user. Nearly all the light reaching the CCD will come from the LED pulses which are offset by a specific time delay relative to the device excitation, and a CCD image is generated as the sum of the LED pulses inside a single CCD exposure window. Figure S1(a) visualizes this process at t = 0 time delay, and S1(b) depicts time-resolved measurements at successive t > 0 time delays.

To create a transient thermoreflectance image, a reference CCD image with LED pulse delay t = 0 is collected, followed by a t > 0 CCD image; then, a subpixel image registration algorithm is applied to a subset of the CCD images to align the t > 0 image to the reference, after which the registered t > 0 image is subtracted from the t = 0 reference. This process with pairs of t = 0, t > 0 images continues as a running average to suppress noise to an acceptable level. In this way the software can automatically step through user-designated time delays and averaging times to collect a full time-domain image set, from the moment the device is turned on, to the time period after the device switches off and is cooling down, all without user involvement.

While this is ongoing, the system periodically checks the current reference CCD image against an initial image taken at the start of the measurement. The system can detect Z-axis sample drift by comparing the sharpness of the initial and current images, and detect XY sample drift by image registration. When it detects sample drift relative to the microscope, it controls an underlying 3-axis piezo nano-positioning stage to compensate so that there is no long-term sample drift, even when collecting and averaging data overnight. With the 250x, 0.9NA objective we have 18 nm/pixel. The piezoelectric stage has <1nm positioning resolution, and with a sub-pixel detection between 0.02-0.04, the system can correct for slow (>1s) drifts down to <1nm in the XY-axis. Positioning in the Z-axis is limited by the depth of focus of the objective to ~10 nm. Instantaneous XY shifts due to vibrations or other movements is corrected for digitally in each frame.
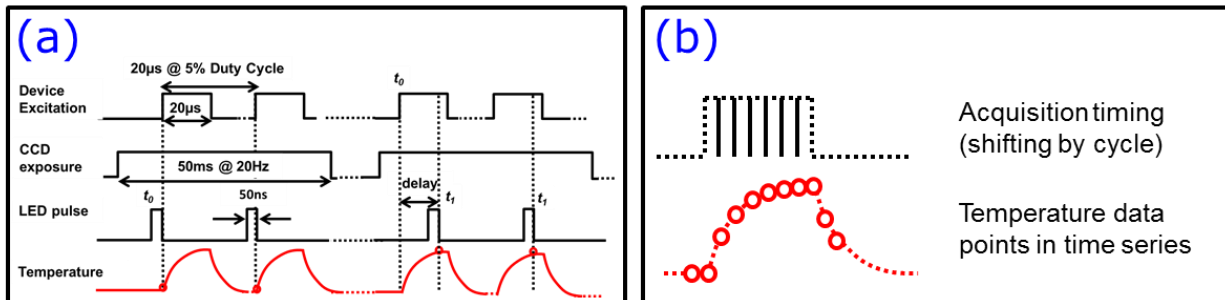
Figure S1 (a) Timing diagram for the pump-probe imaging system: time-resolved image data is collected by pulsing the device excitation and LED probe light at a controllable relative time delay. This diagram shows how the t = 0 data point is collected. **(b)** Inter-locking transient imaging method: Temperature data points are acquired by shifting the timing delay each cycle to achieve a time resolution limited only by how tightly we can pulse the LED probe light.

TCAT: Thermoreflectance Coefficient Analysis Tool

For hot-plate temperature calibration in our system, we place the sample with a thermocouple on a 1 mm tall, 1 cm x 1 cm square Peltier heating stage under the microscope. We then periodically drive the stage to high temperature and back to ambient, and measure the intensity difference between CCD frames in the hot and cold states. All the techniques described above for transient thermal imaging apply, except for TCAT we allow 30-60 seconds per cycle for the stage and sample to reach thermal equilibrium before taking the hot/cold images. The thermoreflectance coefficient is calculated pixel-by-pixel by dividing the change in reflectance by the monitored temperature rise.

In the progression of images in Figure S2, we see that the quality of the resulting thermoreflectance coefficient map depends heavily on how well the system manages thermal expansion induced sample drift and image registration. With a 250x microscope objective, even a modest temperature rise (or return to ambient) will generate a net thermal expansion in the heating stage and sample that far exceeds the depth of focus, so the system must efficiently drive the 3-axis piezo stage to recapture the sample surface and bring it back into alignment before collecting the hot or cold image. Misalignment in X and Y can be corrected for by image registration, but even a small Z focus misalignment between hot and cold images will generate artifacts. See Refs. [1-2] for implementation details.

Artifacts in TCAT are of two origins. First, Dilhaire et al.[3] discovered that a parasitic Fabry-Perot mode can be generated between a very high NA objective lens and the sample surface, such that the observed reflectance is modulated at a scale shorter than the depth of focus. An inconsistency in focal position between hot/cold images can influence the apparent thermoreflectance coefficient, not just near edges.

The second category, edge effects, is most severe for micron and sub-micron features and can arise from poor Z alignment, poor XY image registration, and large scale thermal expansion that slightly changes the size and spacing between features. Figure S2(b) showcases XY image mis-registration artifacts, and S2(e) shows mainly global thermal expansion artifacts, the red patches at the ends of the wearpads. A single nanometer (1/20th of a pixel, here) mis-registration will create major edge effects across the field of view, while global expansion edge effects are magnified away from the reference region for image registration.
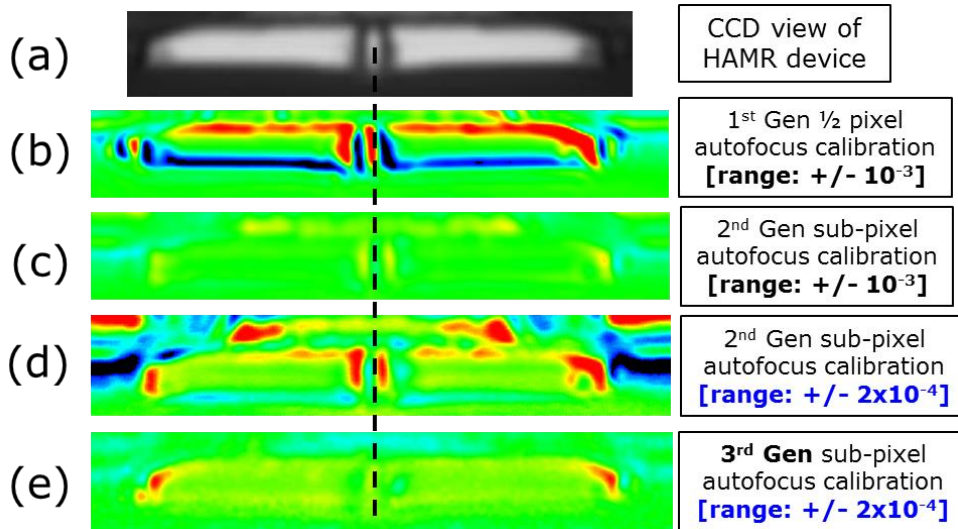
(a)	CCD view of HAMR device
(b)	1st Gen ½ pixel autofocus calibration **[range: +/- 10⁻³]**
(c)	2nd Gen sub-pixel autofocus calibration **[range: +/- 10⁻³]**
(d)	2nd Gen sub-pixel autofocus calibration **[range: +/- 2x10⁻⁴]**
(e)	**3rd Gen** sub-pixel autofocus calibration **[range: +/- 2x10⁻⁴]**

Figure S2 (a) CCD image of HAMR plasmonic device, featuring two wearpads (approx. 1 micron tall) and a central magnetic write pole (approx. 200 nm wide). The plasmonic near-field transducer (NFT) lies immediately below the write pole, but is smaller than 100 nm and not visible under 530 nm LED illumination. **(b)** TCAT thermoreflectance coefficient map; note the saturated red and blue extremes due to imperfect image registration, and how they overwhelm signal (green) from the pole and edges of the wearpads. **(c)** 2nd generation TCAT map with sub-pixel (to 1/50th of a pixel) image registration, same color scale. **(d)** Same as (c), but reduced scale to show that the true C_{th} (of order 5×10^{-5} K⁻¹) is still overwhelmed over the diffraction-limited pole. **(e)** 3rd generation TCAT map, same scale as (d). The symmetry in (e) as opposed to (b) indicates that edge effects are now dominated by global thermal expansion, not image mis-registration. The wearpad thermoreflectance coefficient C_{th} is easily extracted, and the pole C_{th} looks slightly artificial, but similar in magnitude. This is not surprising, since the wearpads and pole are made of the same material.

TCAT: EDGE EFFECTS FROM MIS-REGISTRATION AND GLOBAL THERMAL EXPANSION

There are two sources of edge effect artifacts in TCAT images: imperfect image registration, and global thermal expansion. Because thermoreflectance coefficients are of order 10^{-5} to 10^{-4} K⁻¹, even a sub-nanometer error in image registration will create large edge effects that overwhelm signal from sub-micron areas along the edges of reflective surfaces on the device.

To quantify this claim, we generated a simulated edge effect image based on a CCD image of our device (Figure S3(a)). We applied a simple 3x3 convolution matrix to generate linear fractional shifts in the CCD image along the x- and y-axes, and subtracted the original from the shifted image.

We chose the x- and y-axis shifts so that the simulated edge effects were similar in magnitude to the edge effects we observed from a high-quality, 1st generation TCAT image. As noted in Figure S1(b), the image registration in the 1st generation TCAT software was only good to ½ pixel. The real and simulated TCAT images are shown in Figure S4 (a) and (b), respectively, and the simulated shifts were $\Delta x = +0.030$ pixel, $\Delta y = -0.006$ pixel. With 18 nm /

pixel on our camera, the Δx shift is barely more than 0.5 nm. The 3x3 linear fractional shift matrix in this case was:

$$\begin{bmatrix} 0 & 0.00582 & 0.00018 \\ 0 & 0.96418 & 0.02982 \\ 0 & 0 & 0 \end{bmatrix}$$

Evidently a sub-nanometer shift, on the order of a 10th of a pixel, is enough for the steep brightness gradient along the diffraction-limited edges of metallic features to show an edge effect with magnitude 10x to 100x larger than the thermoreflectance signal. Submicron features such as the central pole (Figure 3a-c) are completely submerged in edge effects and cannot be calibrated in TCAT.

In the latest (3rd generation, Figure 3e) iteration of the TCAT software, image shift related edge effects are minimal, but edge effects due to global thermal expansion remain. Figure S3(b) shows the full TCAT image data from which Figure S2(e) was taken. Edge effects are minimal near the image registration reference region (black rectangle), and are oriented outward with increasing magnitude away from the reference. When the sample heats up on the heating stage, thermal expansion extends the dimensions of components in the field of view, which causes the stretching appearance away from the pinned reference region.

Edge effects are minimal in the reference region, but the TCAT map does not capture the enhanced thermoreflectance along edges that we observe in our raw transient data. So we only use TCAT for the thermoreflectance coefficients of the wearpad interiors, which are unambiguous. We can then use the wearpad interiors as reference thermometers for the transient calibration technique, which addresses the thermoreflectance of diffraction-limited edges and structures.
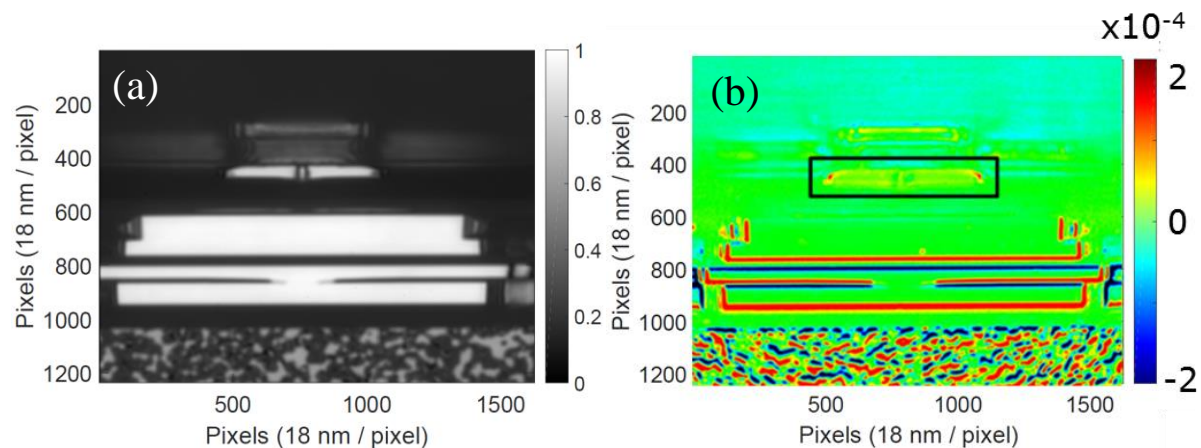

Figure S3 (a) 250x (NA = 0.9) optical CCD image of the HAMR device for the TCAT vs. simulated edge effect comparison. **(b)** Thermoreflectance coefficient map taken with 3rd generation TCAT software with subpixel image registration. Edge effects are horizontally symmetric and oriented away from the wearpad and pole device region, where the image registration reference (black rectangle) was defined. Edge effects are also more severe with increasing distance from the reference region.
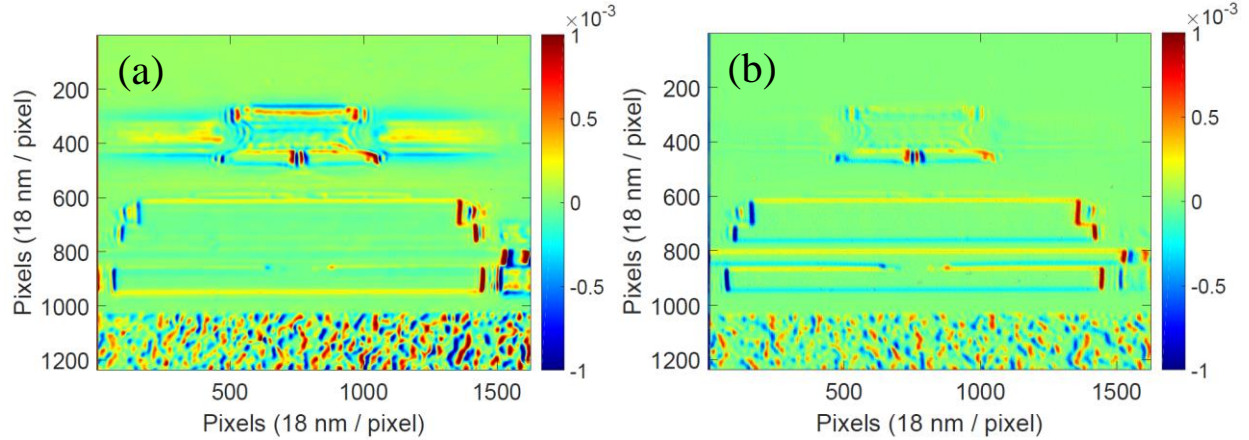
Figure S4 (a) 1st generation TCAT data, collected using 530 nm LED illumination (Thorlabs, ~15 nm FWHM), hot/cold ΔT = 23.8 K, and a 44 s hot/cold cycle period, averaging over 630 cycles. Edge effects here are largely due to flawed image registration, as can be seen in the blue/red asymmetry in left-right and top-bottom edge artifacts, as if reflective surfaces had shifted to the right. **(b)** Edge effect simulation by artificially applying Δx = +0.030 pixels, Δy = -0.006 pixels offset to the CCD image (a), and subtracting the original from the offset image.

TIME SCALE FOR STEADY-STATE TEMPERATURE RISE

As part of the transient calibration process, we need to establish a steady-state temperature rise on the powered device. In Figure S5, we plot the average temperature rise over time of a wearpad interior and the write pole, assuming they have equal thermoreflectance coefficients as suggested by the TCAT data in Figure S2(e). The data and corresponding simulation shows that we can reach local steady-state heating by powering the device for 20 μs.

POLARIZATION-DEPENDENCE IN NANOSCALE THERMOREFLECTANCE

The plasmonic thermoreflectance response of our sub-micron metallic structure manifests as a polarization dependence of the thermoreflectance signal. Because the HAMR near-field transducer (NFT) and surrounding metals have different dimensions along the x- and y-axes of our imaging system, x- and y-polarized light from the microscope's LED will be more or less distant from a plasmon resonance peak, with a corresponding difference in the measured thermoreflectance signal. Figure S6 shows variations in the raw thermoreflectance signal due to inserting vertical and horizontal polarization filters in the probe path. Note that our thermoreflectance signal is $\Delta R/R$, not the absolute ΔR, so any differences in illumination intensity or reflectance R between the two polarizations are normalized out.
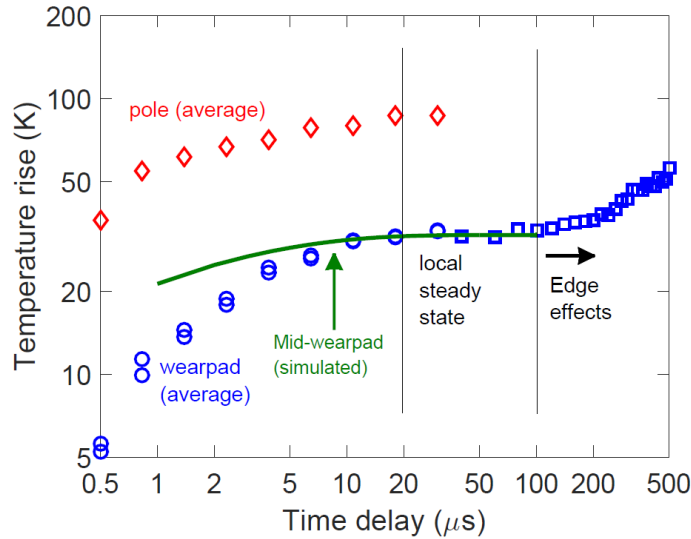
Figure S5 Demonstration that the HAMR device reaches local steady-state after 20 μs of excitation. The green curve is a simulated, rescaled temperature rise at the midpoint of the wearpad. The wearpad average data points (blue circles, squares) lag below the simulation because the wearpad average data includes the far ends, which take longer to heat up. Beyond 100 μs, edge-effect artifacts crept into the wearpad region, much like in the TCAT data shown in Figure S2(b). The onset of edge effects would be later in the current version of the system's software.
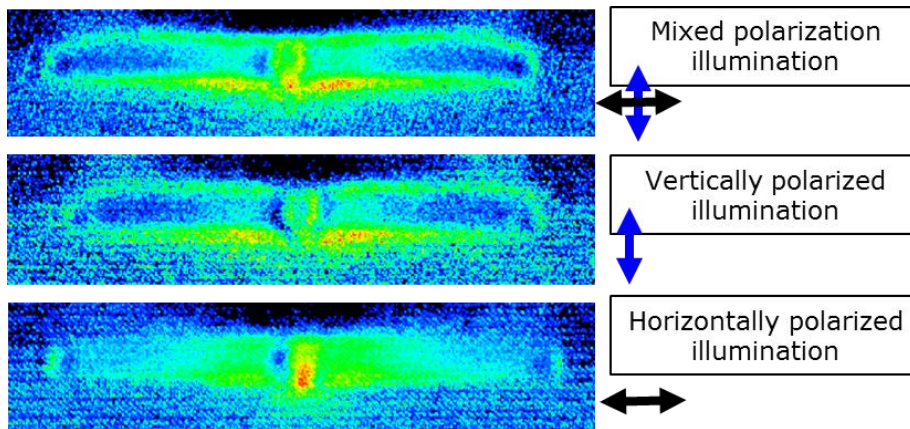

Figure S6 The observed thermoreflectance signal for three different polarization states of the 530 nm LED probe illumination. This is not the same device or averaging time as for other figures. Vertical and horizontal polarizations were generated by inserting a linear polarizer in front of the LED. The mixed polarization state was just the LED without filters; the horizontal and vertical components were similar but not equal in magnitude. Broadly, the thermoreflectance appears enhanced where the polarization is aligned with the short dimension of a visible structure.

SUPPLEMENTARY REFERENCES

1. K. Yazawa, D. Kendig, K. Al-hemyari, A. Shakouri, *Proc. ITHERM*, 1308 (2014).
2. A. Shakouri, A. Ziabari, D. Kendig, J.-H. Bahk, Y. Xuan, P. D. Ye, K. Yazawa, and A. Shakouri, *Proc. SEMI-THERM*, 128-132 (2016).
3. S. Dilhaire, S. Grauby, and W. Claeys, *Appl. Phys. Lett*. 84, 822 (2004).